PERMITTIVITY PROBE MODELLING

Camelia Gabriel

Department of Physics
King's College London
Strand, London WC2R 2LS, UK

OCCUPATIONAL AND ENVIRONMENTAL
HEALTH DIRECTORATE
Brooks Air Force Base, TX 78235-5000

November 1991

Final Technical Report for Period September 1989 – July 1990

AIR FORCE SYSTEMS COMMAND
BROOKS AIR FORCE BASE, TEXAS 78235-5000

ARMSTRONG LABORATORY

NOTICES

When Government drawings, specifications, or other data are used for any purpose other than in connection with a definitely Government-related procurement, the United States Government incurs no responsibility or any obligation whatsoever. The fact that the Government may have formulated or in any way supplied the said drawings, specifications, or other data, is not to be regarded by implication, or otherwise in any manner construed, as licensing the holder or any other person or corporation; or as conveying any rights or permission to manufacture, use, or sell any patented invention that may in any way be related thereto.

The Office of Public Affairs has reviewed this report, and it is releasable to the National Technical Information Service, where it will be available to the general public, including foreign nationals.

This report has been reviewed and is approved for publication.

William D. Hurt

WILLIAM D. HURT, M.S.
Project Scientist

David N. Erwin

DAVID N. ERWIN, Ph.D.
Chief, Radiofrequency Radiation Branch

Michael L. Dinion

MICHAEL L. DINION, Lt Col, USAF, BSC
Chief, Directed Energy Division

REPORT DOCUMENTATION PAGE

Form Approved
OMB No 0704-0188

1. AGENCY USE ONLY (Leave blank)	2. REPORT DATE	3. REPORT TYPE AND DATES COVERED
	November 1991	Final Sep 1989 - Jul 1990

4. TITLE AND SUBTITLE

Permittivity Probe Modelling

5. FUNDING NUMBERS

C - F33615-87-D-0626-0009
PE - 62202F
PR - 7757
TA - 01
WU - 2F

6. AUTHOR(S)

Camelia Gabriel

7. PERFORMING ORGANIZATION NAME(S) AND ADDRESS(ES)

Department of Physics
King's College London
Strand, London WC2R 2LS, UK

8. PERFORMING ORGANIZATION REPORT NUMBER

9. SPONSORING / MONITORING AGENCY NAME(S) AND ADDRESS(ES)

Armstrong Laboratory
Occupational and Environmental Health Directorate
Brooks Air Force Base, TX 78235-5000

10. SPONSORING / MONITORING AGENCY REPORT NUMBER

AL-TR-1991-0055

11. SUPPLEMENTARY NOTES

Armstrong Laboratory Technical Monitor: William D. Hurt, (512) 536-3185

12a. DISTRIBUTION / AVAILABILITY STATEMENT

Approved for public release; distribution is unlimited.

12b. DISTRIBUTION CODE

13. ABSTRACT *(Maximum 200 words)*

An HP 8720 automatic network analyser has been used with a custom made coaxial probe to measure the complex permittivity of standard liquids in the frequency range 130 MHz to 20 GHz. Three equivalent circuit models were used to simulate the admittance of the probe sample interface. The expediency and limitations of these models have been studied. A critical review of these simulations is presented and illustrated by experimental evidence. Measurements were performed on high and low loss materials to test the power and versatility of the adopted technique. Its accuracy and reproducibility compare favourably with the well established, in-guide, techniques. This technique is well suited for applications in the fields of biomedicine, material studies and industrial development and control.

14. SUBJECT TERMS	15. NUMBER OF PAGES
Permittivity probe modelling; Coaxial probe modelling; Admittance model; Finite element technique; Static fringing electric field.	46
	16. PRICE CODE

17. SECURITY CLASSIFICATION OF REPORT	18. SECURITY CLASSIFICATION OF THIS PAGE	19. SECURITY CLASSIFICATION OF ABSTRACT	20. LIMITATION OF ABSTRACT
Unclassified	Unclassified	Unclassified	UL

TABLE OF CONTENTS

A-1

PERMITTIVITY PROBE MODELLING

1. INTRODUCTION

The use of the open-ended probe for measurements requires a semi-infinite sample to be placed in contact with it. To define, in practical terms, the extent of the sample we have recently developed a finite element technique to model the fringing fields of open-ended lines and their perturbation by a material. The current technique accommodates lossless dielectric; its extension to lossy materials will be briefly outlined.

Numerous papers have reported the use of open-ended coaxial lines for dielectric measurements at microwave frequencies (1-4). The technique is based on the study of the fringing admittance of the open-ended line and its alteration by a lossy dielectric. The system is nondestructive; its advantages are of a practical nature mainly associated with the simple handling of samples. The principal shortcoming of the technique is that a full analysis of the end-of line-admittance requires extensive numerical calculation and does not lend itself to real-time measurements (5) while simple models that assume the probe to be nonradiating and only capacitive in nature fail progressively at high frequency and for lossy materials. In this report we introduce 2 approximate admittance models in which the radiating element of the probe is explicitly treated together with inductive and capacitive components. The models will be expressed in a polynomial form suitable for a numerical solution so that the complex permittivity of the sample in contact with the probe is calculated from the measured values of the admittance. A comparative study of the performance of all 3 models is included. Results show that the 2 new models, derived from the same set of assumptions, are not equal in performance. The better of the 2 models is used in conjunction with a 3-mm probe and a Hewlett Packard (HP) 8720 network analyzer for dielectric measurements on standard liquids. The results show that the technique is suitable for measurements on lossy materials to 20 GHz. Its accuracy and precision are assessed by comparing the measurements with equivalent values from the literature.

2. COAXIAL PROBES MODELLING

A second order polynomial finite element technique was developed in 1988 in our research group (6) to model the fringing capacitance of coaxial probes. The implementation of the technique requires that the area of the solution be divided into a mesh of triangular elements. The potential of both the inner and outer conductors is known and assumed constant. The potential in each triangular element is approximated by a function the coefficient of which is related to the spatial coordinates of the element. Minimisation of the potential energy of the system yields an approximation of the potential distribution that satisfies Laplace's equation.

For the purpose of this application a coaxial air line of inner and outer radii a and b respectively is represented as in Figure 1.

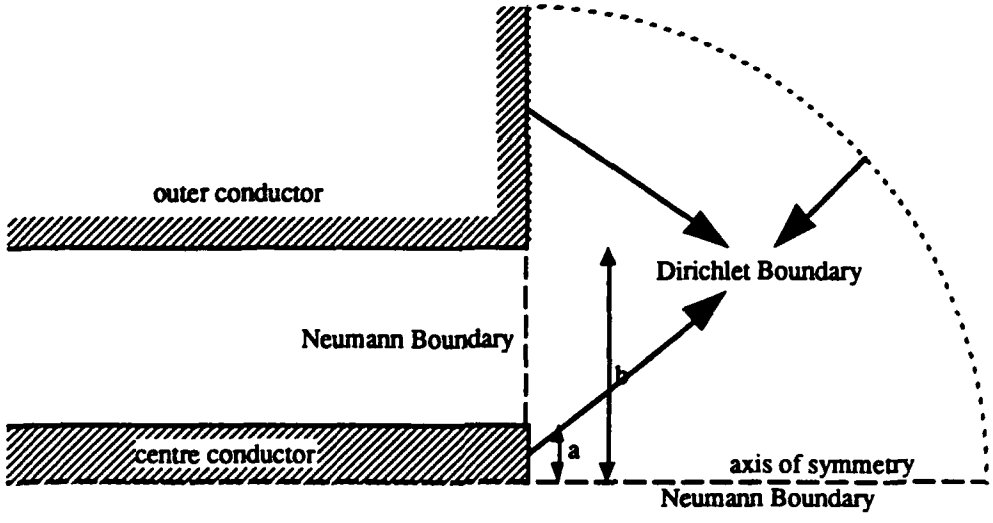

Figure 1. Region in which the solution is implemented.

The technique was extensively improved in the course of the current project. In particular, an automatic mesh generator was developed and the solution used to plot equipotential lines in the area under study.

2.1 Implementation of the Solution

The region of the solution is divided into triangular elements. The mesh is partially bounded by Dirichlet and Neumann boundaries Figure 1.

The inner and outer conductors are held at 1 and 0 volts respectively.

In each element the relative permittivity ε_k is known and the potential Φ is approximated by a trial function with constant coefficients, such that

$$\phi = \sum_{i=1}^{3} \alpha_i \phi_i \tag{1}$$

where Φ_i is the potential at vertex i and α_i is a linear expression in r and z, the vertex coordinates.

In terms of these elements the potential energy stored in the region of the solution is proportional to

$$F = \sum_{k=1}^{no\ of\ elem} 2\Pi\, \varepsilon_k \int_{r_k, z_k} (\nabla \phi)_k^2\, r\, dr\, dz \tag{2}$$

where r_k is the radial component of each element. The finite element method was implemented to the second order so that each triangle is defined by 6 nodes.

Combining Equations 1 and 2 we obtain

$$F = 2\pi \sum_{k=1}^{no\ of\ elem} \varepsilon_k \sum_{i=1}^{3}\sum_{j=1}^{3} \phi i \int_{k=1} \nabla \alpha_j \nabla \alpha_j \phi_j\, r\, dr\, dz \tag{3}$$

By minimizing Equation 3 with respect to Φ a set of equations is formed which can readily be solved for the potential at each node.

Equipotential lines are then drawn to give a visual representation of the fringing field of the probe and its perturbation by a dielectric medium.

To test the validity of the model the fringing capacitance of the probe may be calculated using the solution obtained from the model

$$C = \frac{2\pi}{V^2}\int_{r_s} \varepsilon_0 \varepsilon (\nabla\phi)^2 \, r \, dr \, dz \tag{4}$$

$$= \frac{\varepsilon_0 F_{sol}}{V^2} \tag{5}$$

A comparison between the calculated and measured value of the capacitance validates this approach to the problem.

2.2 Automatic Mesh Generator

At the onset of this project the creation of a triangular mesh to implement the finite element technique was done by hand before each calculation. This procedure is time consuming and prone to error particularly when a finer mesh is required to improve the resolution of the model. A brief or otherwise unsuitable mesh design could lead to inaccurate results. To overcome these difficulties and speed up the process, an automatic mesh generator was developed.

A brief mesh, referred to as the basis mesh, is made in the region of solution and the potential at each node is calculated using the Finite Element approximation. The basis mesh needs refining particularly in the regions of high field gradient. This refining is accomplished by comparing the average potentials of adjacent elements. If the difference is greater than a predefined limit, a node in both of the 2 elements is specified using the angle bisector method.

Connecting this node to the 3 vertices, the corresponding triangular element is subdivided into 3 triangles which are then assigned with new element numbers. After all the elements in the problem are compared, the calculation is carried out again in the new mesh. These procedures are continued until the differences in potential between each adjacent elements are less than the set limit. A brief mesh with 10 elements is shown in Figure 2 and the subdivision of elements 3 and 8 is shown as an example.

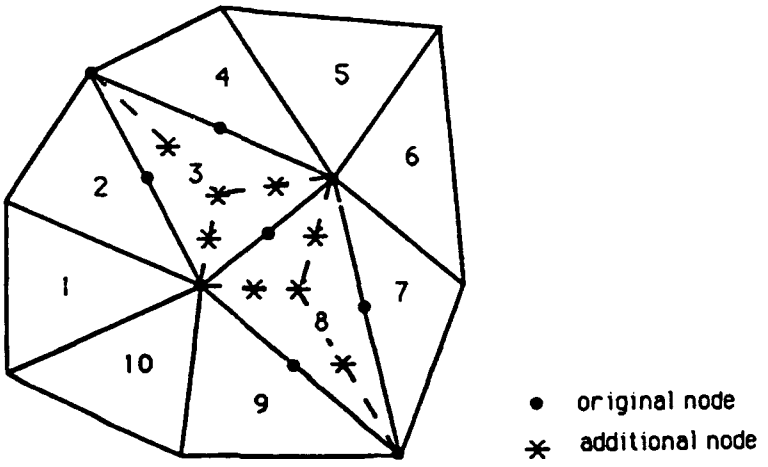

Figure 2. The subdivision of elements 3 and 8 by the angle bisector method.

The basis mesh can also be segmented by another technique, namely the fractal segmentation. In this method, 3 nodes are defined at the midpoints of each side of a triangular element. Connecting these nodes together, 4 equivalent triangular elements are formed which are similar to the original element. The method is illustrated in Figure 3. However, unlike the former technique, this segmentation must be applied to all elements in the system at the same time to satisfy the boundary conditions of adjacent elements. Hence after applying the segmentation once, the number of elements in the new mesh is four times that of the original one.

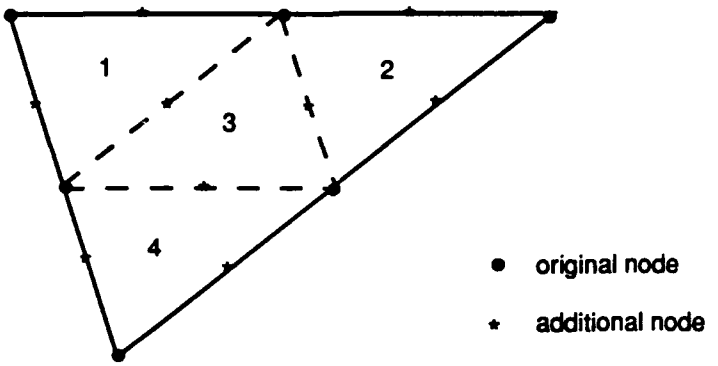

Figure 3. A second order element is subdivided into 4 equivalent elements by the fractal segmentation technique.

2.3 Equipotential Contour Plot

Results are given in Figures 4 - 7. Figure 4 demonstrates the potential due to an open-ended air line. The same technique was used to generate the equipotential lines of a measuring probe based on a Teflon-filled line (Fig. 5), an air line terminated by an impedance matched dielectric window (Fig. 6) and a conical probe of our own design (Fig. 7). This latter probe (UK patent application 882681.1) was designed to provide deeper penetration and to increase the sensitivity of measurements at frequencies below 100 MHz.

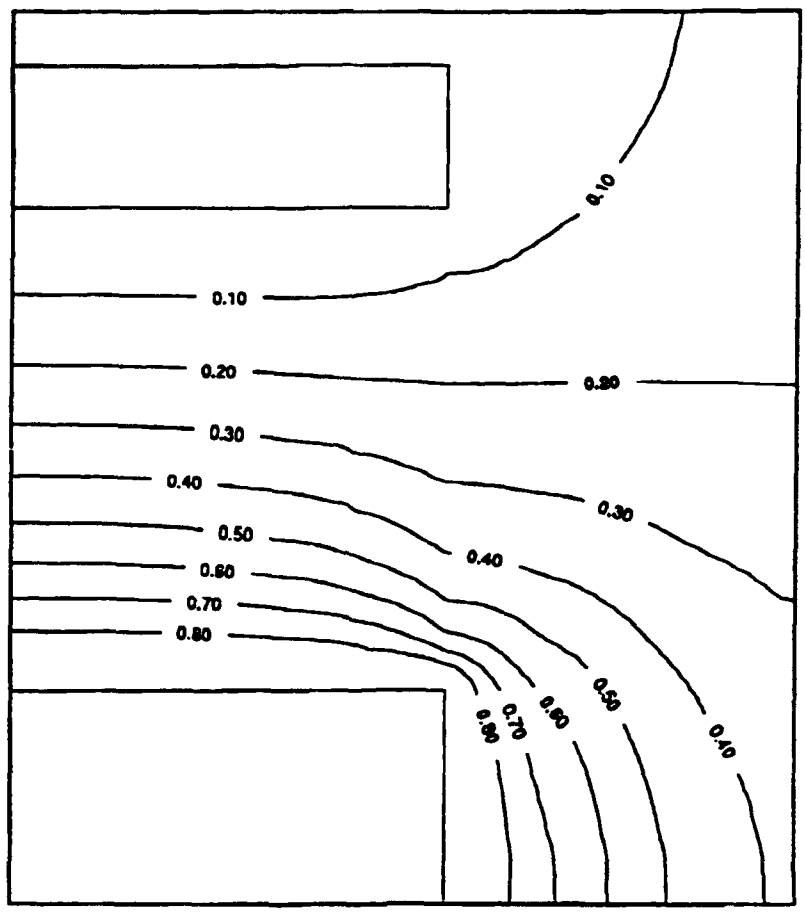

Figure 4. A 0.5 mm inner conductor radius, air line radiating into a dielectric of ε=200.

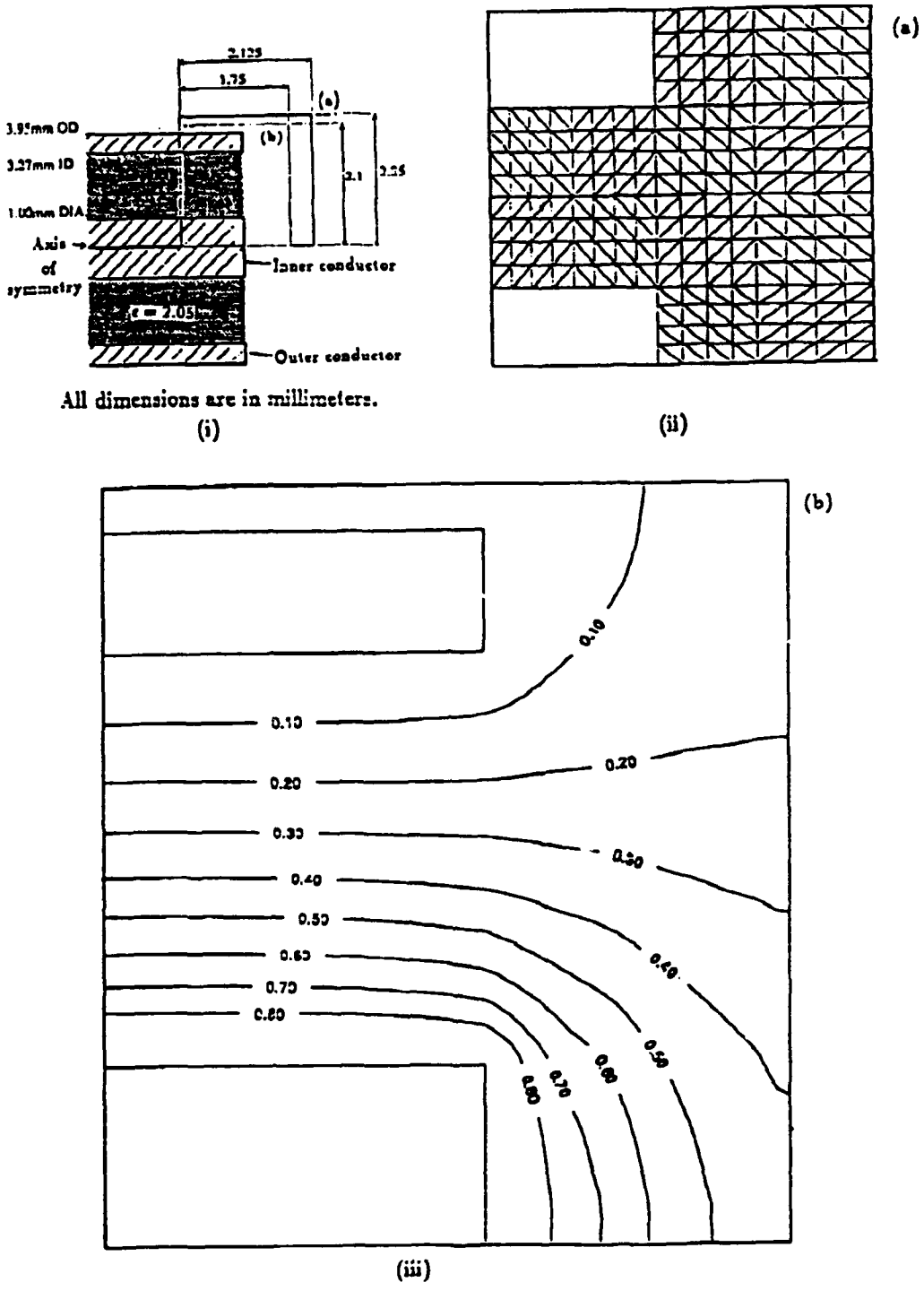

Figure 5. A Teflon filled-line (i) basic configuration and dimensions, (ii) the mesh used in region (a), (iii) the equipotential plot in region (b).

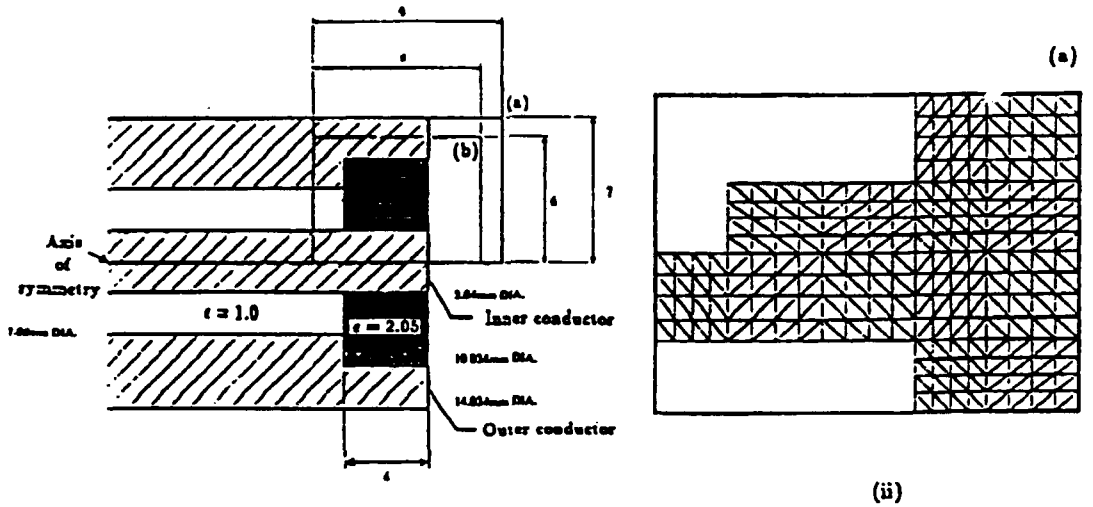

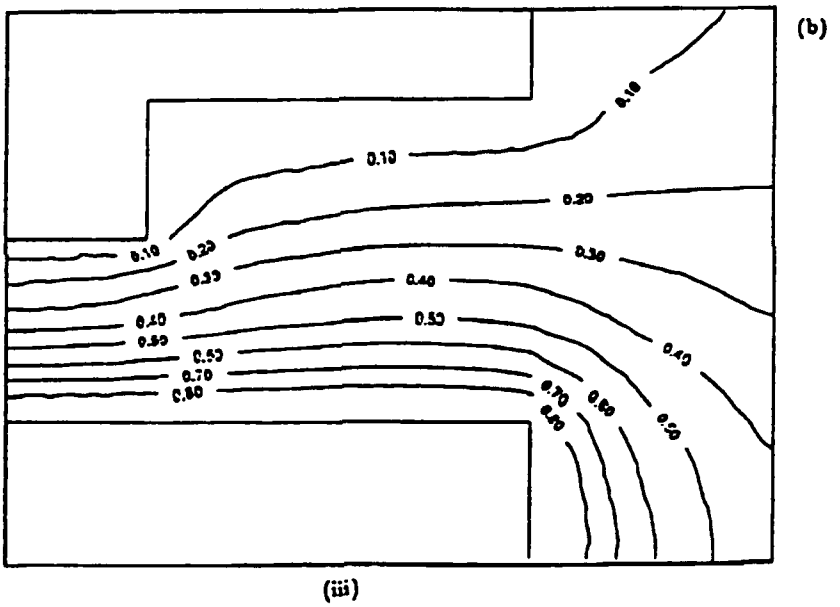

Figure 6. A probe with internal discontinuity (i) basic configuration and dimensions, (ii) the mesh used in region (a), (iii) the equipotential plot in region (b).

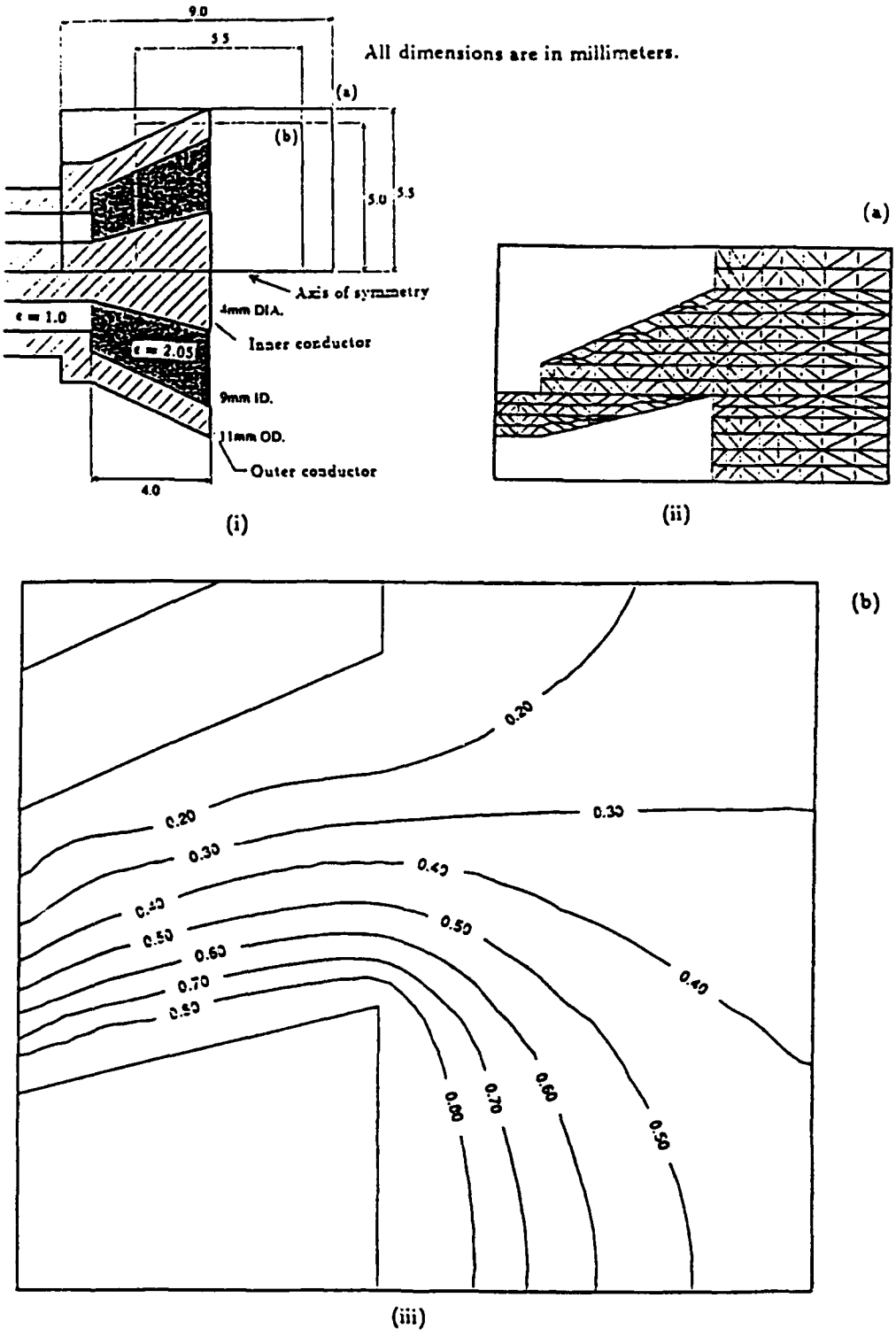

Figure 7. A conical probe (i) basic configuration and dimensions, (ii) the mesh used in region (a), (iii) the equipotential plot in region (b).

2.4 Fringing Fields in Lossy Media

In Figures 4-7 the medium in contact with the probe was assumed real (ε'=constant, $\varepsilon'' = 0$). The extension of the technique to lossy media ($\varepsilon'' \neq 0$) falls outside the scope of this project but will be briefly outlined. If the electric field E is expressed as the gradient of a scaler potential

$$E = - \nabla\phi \tag{6}$$

Then the case of a harmonic field Ampere's Law will be

$$\nabla \times H = - (\sigma + j\,\varepsilon^*\omega)\,\nabla\phi \tag{7}$$

where H is the magnetic field, σ the conductivity , ε the permittivity and ω the radial frequency. Taking the divergence of the above equation gives

$$(\sigma + j\,\varepsilon^*\omega)\,\nabla^2\phi = 0 \tag{8}$$

which can be solved using our existing finite element technique in conjunction with the newly developed automatic mesh generator. This extension to our programme would enable the study of field penetration in lossy homogeneous and layered media. This extension would also be particularly useful in defining the electric field penetration while performing *in vivo* measurements.

3. DEVELOPMENT OF AN ADMITTANCE MODEL

3.1 Theoretical Background

When vector network analyzers are used to characterise the admittance of open-ended coaxial probes,it is inherently assumed that their characteristics at a given frequency and under steady state conditions are indistinguishable from the characteristics of a linear network (i.e., a combination (series or shunt) of a resistor and an inductor or capacitor).

In the case of an open-ended probe the appropriate configuration is capacitive susceptance B in parallel with a conductance G. In this case, it is more convenient to express its equivalent impedance in terms of its inverse, the admittance Y, thus

$$Y = G + jB \tag{9}$$

where G and B are a factor of the propagation constant k and the radial dimensions of the line. By definition the complex reflection coefficient of the probe Γ is given in terms of this admittance as

$$\Gamma = (1-Y/Yo)/(1+Y/Yo) \tag{10}$$

Yo (= 1/Zo) is the intrinsic admittance of the line. The complex reflection coefficient Γ is readily measurable using the experimental setup. The emphasis of the problem at this stage is the relationship of the admittance Y to the complex permittivity ε^* of the sample with which it is in contact. This contact is the relationship that will enable ε^* to be calculated from measured values of Γ or Y.

The relationship between Γ and ε^* is rather complex and a rigorous analytical expression is not available. Several authors have obtained approximate solutions to this problem. The most complete analysis is that of Mosig et al.(5), who calculated the admittance of the open-ended line by matching the electromagnetic fields at the plane of the aperture incorporating the fundamental transverse electromagnetic (TEM) and higher order modes. This approach while limited by certain assumptions is the most accurate model available for an end of line

admittance. However, this analysis cannot be performed on a microcomputer for measurements in real time. Three alternative models have been studied.

3.1.1 Equivalent circuit model (Model 1)

The approach adopted in the first instance is to consider Y in terms of its lumped equivalent circuit parameters The susceptance B is capacitive made up of internal and external fringing fields (Fig. 8):

$$Y = G + j\omega (C_f + C_o(\varepsilon' - j\varepsilon'')) \tag{11}$$

where C_f and C_o are the components of the fringing field, ω is the angular frequency (rad/sec) and $\varepsilon^* = \varepsilon' - j\varepsilon''$ is the complex permittivity of the sample.

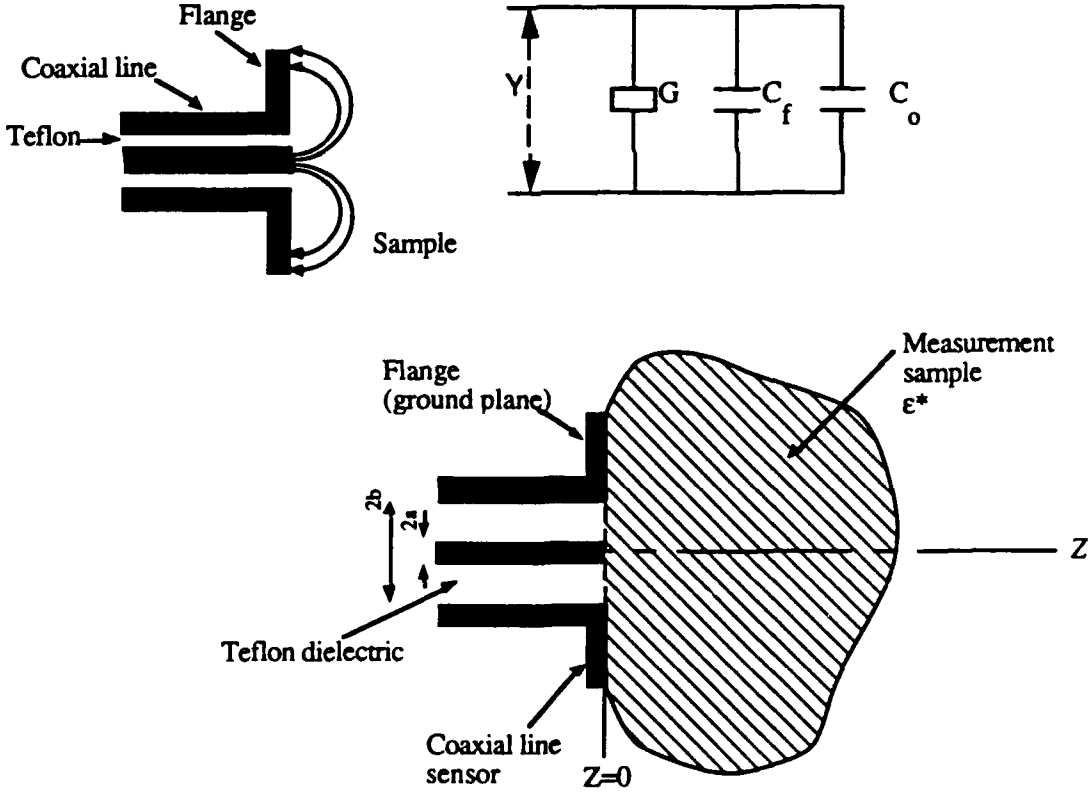

Figure 8. Model 1 approximation of the coaxial probe.

At the limit of low frequencies G=0 and C_f and C_o are constants that depend on the dimensions of the probe.

Assuming the probes are used at frequencies such that the wavelength of the propagating wave is significantly larger than the radial dimensions of the probe, a quasi-steady state would prevail. From these equations we would have:

$$\Gamma = (1 - j\omega Z_o(C_f + C_o \varepsilon^*)) / (1 + j\omega Z_o(C_f + C_o \varepsilon^*)) \quad (12)$$

and

$$\varepsilon^* = (1- \Gamma) / (j\omega C_o Z_o(1+ \Gamma)) - C_f/C_o \quad (13)$$

with C_f significantly smaller than C_o. Neglecting the contribution of C_f to the permittivity would introduce an error in ε^*. This error has been shown to be small compared to the value of ε^* of most biological samples at radio and microwave frequencies. This led some authors to simplifying the equivalent circuit of the open-ended probe to a single shunt capacitance C_o (1). In this case the reflection coefficient becomes

$$\Gamma = (1- jwC_o Z_o \varepsilon^*) / (1+ jwC_o Z_o \varepsilon^*) \quad (14)$$

Implementation of Model 1

Our approach to the problem at this stage is to consider the general case (Equation 11) and assume the following:

- G and C_f contribute to the admittance of the probe.
- Their contribution is significantly less than that of the external fringing capacitance C_o,
- Their contribution may exhibit a certain degree of frequency dependence and to a lesser extent a dependence on ε^*, and
- C_o may also exhibit some dependence on frequency and ε^*.

These assumptions lead us to express the measured reflection coefficient Γ_m as:

$$\Gamma_m = \Gamma(\omega, C_o, \varepsilon^*) + F(\omega, C_o, \varepsilon^*, C_f, G) \tag{15}$$

Under certain conditions, notably when the wavelength of the source is much larger than the radial dimensions of the probe, the correction term F is small and of the order of magnitude of the experimental uncertainty. It is, however, good experimental practice to eliminate it from the measured parameter. The corrected reflection coefficient Γ may then be solved for ε^*.

Our approach to this correction is to use the response of a reference sample and a difference technique (4) to normalise the unknown response.

3.1.2 Integral expression of the admittance (Model 2)

In the cylindrical coordinate system (ρ, ϕ, z), Figure 9, assuming the radial electric field intensity over the aperture $E_\rho(\rho,0)$ is inversely proportional to ρ, an expression for aperture admittance can be obtained (7,8).

$$\overline{Y_L} = j\frac{k^2}{\pi k_c \ln(b/a)} \int_a^b \int_a^b \int_0^\pi \cos\phi' \frac{\exp(-jkr)}{r} d\phi' d\rho' d\rho \tag{16}$$

where :

$$k^2 = \omega^2 \mu_o \varepsilon^*$$

$$k_c^2 = \omega^2 \mu_o \varepsilon_c \varepsilon_o$$

$$r^2 = \rho^2 + \rho^2 - 2\rho\rho' \cos\phi'$$

$$Y_o = 2\pi\left[\sqrt{\frac{\mu_o}{\varepsilon_o\varepsilon_c}}\ln\frac{b}{a}\right]^{-1} \qquad (17)$$

The dielectric window is assumed lossless of permittivity ε_c, ε^* is the complex permittivity of a semi-infinite sample.

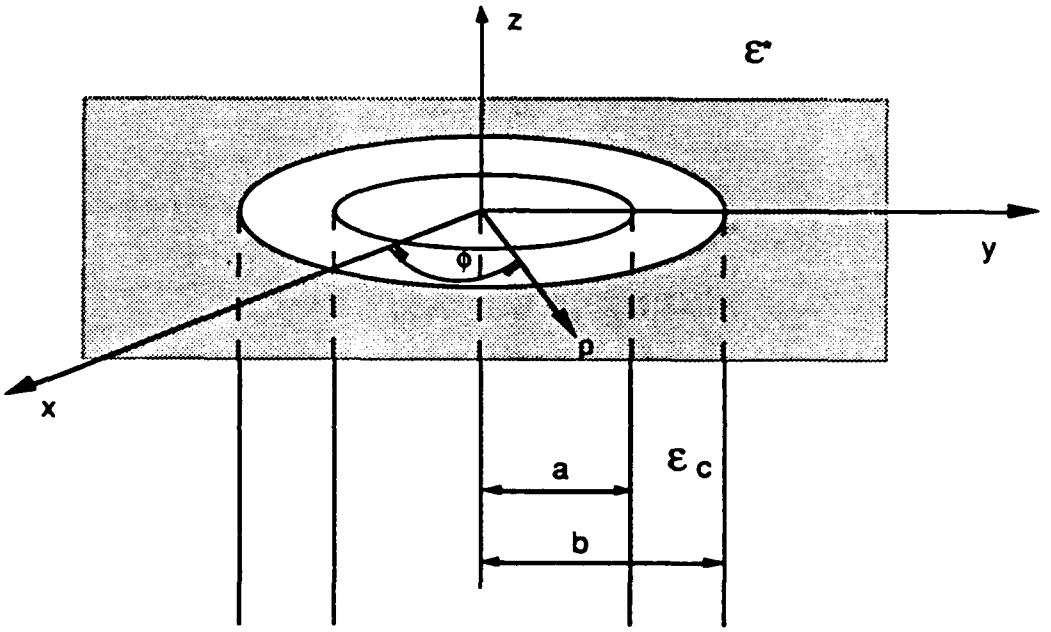

Figure 9. Schematic representation of the coaxial probe in terms of the parameters of Model 2 and Model 3.

Misra (7) has shown that when the radial dimensions of the probe are much smaller than the propagating wavelength Equation (16) can be approximated by the first terms of the series expansion for the exponential term and used to calculate ε^*, numerically, from measured values of Y. This approximation was found suitable for the measurement of low permittivity materials.

Implementation of Model 2

Substituting equation (17) into (16) and expanding the exponential term into an infinite series, Y can be expressed as

$$Y = \omega C_o\{\varepsilon^* C_1 + \varepsilon^{*2} C_3\omega^2 + \varepsilon^{*5/2} C_4\omega^3 + \varepsilon^{*3} C_5\omega^4 + \varepsilon^{*7/2} C_6\omega^5 + \varepsilon^{*4} C_7\omega^6 + \varepsilon^{*9/2} C_8\omega^7 + \varepsilon^{*5} C_9\omega^8 + \varepsilon^{*11/2} C_{10}\omega^9 + \ldots\} \quad (18)$$

where:

$$C_0 = j\frac{2}{[\ln(b/a)]^2}$$

$$C_1 = \int_a^b\int_a^b\int_0^{\pi} \frac{\cos\phi'}{[\rho^2+\rho'^2-2\rho\rho'\cos\phi']^{1/2}} d\phi' d\rho' d\rho$$

$$C_3 = -\frac{1}{2}\mu_o \int_a^b\int_a^b\int_0^{\pi} \cos\phi'[\rho^2+\rho'^2-2\rho\rho'\cos\phi']^{1/2} d\phi' d\rho' d\rho$$

$$C_4 = -j\frac{\pi}{24}(b^2-a^2)\mu_o^{3/2}$$

$$C_5 = \frac{\mu_o^2}{24}\int_a^b\int_a^b\int_0^{\pi} \cos\phi'[\rho^2+\rho'^2-2\rho\rho'\cos\phi']^{3/2} d\phi' d\rho' d\rho$$

$$C_6 = -j\frac{\pi}{240}(b^2-a^2)(b^4-a^4)\mu_o^{5/2}$$

$$C_7=\frac{\mu_o^3}{720}\int_a^b\int_a^b\int_0^{\pi}\cos\phi'[\rho^2+\rho'^2-2\rho\rho'\cos\phi']^{5/2}d\phi'd\rho'd\rho$$

$$C_8=-j\frac{\pi\mu_o^{7/2}}{3360}[\frac{(b^6-a^6)(b^2-a^2)}{3}+\frac{3}{8}(b^4-a^4)^2]$$

$$C_9=\frac{\mu_o^4}{40320}\int_a^b\int_a^b\int_0^{\pi}\cos\phi'[\rho^2+\rho'^2-2\rho\rho'\cos\phi']^{7/2}d\phi'd\rho'd\rho$$

The second term of the series expansion goes to zero on integration over ϕ'. Since the integrand of C_1 is singular at $\rho = \rho'$ for $\phi' = 0$, it is calculated analytically and can be expressed as

$$C_1 = 4(a+b)[E(m) - 1] \tag{19}$$

where E(m) is the complete elliptic integral of the second kind, which can be approximated by a polynomial (12), and

$$m = \frac{4ab}{(a+b)^2} \tag{20}$$

Since C_i, where $i = 0, ..., 10$, are dependent only on the physical dimensions of the aperture, they can be evaluated for a given coaxial line. The triple integrals are performed numerically by Simpson's three points rule. The intervals [a,b] and [o,π] are subdivided into 2N (=10) subintervals and Simpson's rule is applied on each pair of consecutive subintervals. The maximum tolerance in the calculation of E(m) was set to be 10^{-20}. The number of terms in the series in Equation (18) was varied between 3 and 20 to allow a check for convergence and accuracy in the model. The values of C_i, where $i = 0, ..., 20$, were calculated for a 50 Ω 3-mm OD probe. These values were then substituted into equation (18) and the probe admittance Y was evaluated from 130 MHz to 20 GHz. As the number of C_i terms considered was increased

the calculated value of the admittance converged to a constant value when nine terms in the series expansion were included.

Implicit in this model is that only the lowest transmission mode, the TEM mode, is propagated. Although this mode is the dominant mode, higher order modes will be generated at the probe sample interface.

In a measurement situation a Newton-Raphson technique is used to calculate the complex permittivity of the sample from the experimentally measured values of Y at each frequency of interest.

During the development of the model the network analyzer was calibrated using factory standards before fitting the probe.

3.1.3 Integral expression of the admittance (Model 3)

Another equivalent formulation for the admittance of the line is also given by Marcuvitz as (8)

$$Y = G + jB \tag{21}$$

$$G = \frac{Y_o \sqrt{\varepsilon^*}}{\ln(b/a)\sqrt{\varepsilon_c}} \int_o^{\pi/2} \frac{1}{\sin\theta} \left[J_o\left(k_o \sqrt{\varepsilon^* b \sin\theta}\right) - J_o\left(k_o \sqrt{\varepsilon^* a \sin\theta}\right) \right]^2 d\theta \tag{21a}$$

$$B = \frac{Y_o \sqrt{\varepsilon^*}}{\pi \ln(b/a)\sqrt{\varepsilon_c}} \int_o^{\pi} \left[2Si\left(k_o \sqrt{\varepsilon^* \left(a^2 + b^2 - 2ab\cos\theta\right)}\right) - 2Si\left(2k_o \sqrt{\varepsilon^* a \sin\left(\frac{\theta}{2}\right)}\right) - 2Si\left(2k_o \sqrt{\varepsilon^* b \sin\left(\frac{\theta}{2}\right)}\right) \right] d\theta \tag{21b}$$

where k_o is the propagation constant in free space, ω/c, where c is the velocity of light in vacuum and ω is the angular frequency; J_o is the Bessel function of order zero; and Si is the sine integral.

Equations 21a and 21b represent an expression of the admittance of a probe as an integral over its aperture. This approximation was also studied by Levine and Papas (9), Xu *et al.*(10) and Misra *et al.* (11) and was derived by Misra (7) as Equation (18). Therefore, Model 2 and 3 are equivalent to each other. Both models were obtained from a variational expression for the input admittance of a coaxial cable opening into an infinite ground plane and semi-infinite sample dielectric. The variational expression was written in terms of an integral equation for the unknown electric field distribution in the aperture and was solved using the principal (TEM) mode of the coaxial guide to represent the aperture field. Thus the solutions given by Equations 8 and 21a and 21b do not take into account the excitation of higher-order modes in the aperture.

Implementation of Model 3

Since the Bessel function of order zero and the sine integral can be expressed in series expansions,

$$J_o(z)=\sum_{p=0}^{\infty}\frac{(\frac{1}{4}z^2)^p}{(p!)^2} \tag{22}$$

$$Si(z)=\sum_{p=0}^{\infty}\frac{(-1)^p z^{2p+1}}{(2p+1)(2p+1)!} \tag{23}$$

Equations (21a) and (21b) become

$$B=\sum_{n=0}^{\infty}\frac{1}{\pi}K_1K_2^{(2n+1)}I(n)f^{(2n+1)}\varepsilon^{*(n+1)} \tag{24}$$

$$G=K_1\left\{\sum_{p=1}^{\infty}\sum_{q=1}^{\infty}\frac{\varepsilon^{*(p+q+\frac{1}{2})}f^{2(p+q)}(-\frac{1}{4}K_2^2)^{p+q}(b^{2p}-a^{2p})(b^{2q}-a^{2q})S(p+q-1)}{2(p!q!)^2}\right\} \tag{25}$$

where:

$$K_1=\frac{1}{Z_o\ln(b/a)\sqrt{\varepsilon_c}} \tag{26}$$

$$K_2=2\pi/c \tag{27}$$

$$I(n) = \frac{(-1)^n}{(2n+1)(2n+1)!}\left\{\int_0^{\pi} 2(a^2+b^2-2ab\cos\theta)^{(n+\frac{1}{2})}d\theta-(a^{2n+1}+b^{2n+1})2^{2n+1}S(n)\right\} \tag{28}$$

$$S(n)=\int_0^{\pi} \sin^{2n+1}(\frac{\theta}{2})d\theta \tag{29}$$

Equations (24) and (25) can then be rearranged to be--

$$B=\sum_{n=0}^{\infty} F_b(n)\varepsilon^{*(n+1)}f^{(2n+1)} \tag{30}$$

$$G=\sum_{p=1}^{\infty}\sum_{q=1}^{\infty} F_g(u)\varepsilon^{*(p+q+\frac{1}{2})}f^{2(p+q)} \tag{31}$$

where:

$$F_b(n)=\frac{1}{\pi}K_1K_2^{(2n+1)}I(n) \tag{32}$$

$$F_g(u)=\frac{K_1(\frac{1}{4}K_2^2)^{p+q}(b^{2p}-a^{2p})(b^{2q}-a^{2q})S(p+q+1)}{2(p!q!)^2} \tag{33}$$

$$u = p+q-2 \tag{34}$$

It can be noted that arrays F_b and F_g are functions of a and b only and can be evaluated for a given coaxial sensor. The integral in I(n) was performed by Simpson's three point rule with 100 subintervals. Moreover, a subroutine was written to evaluate S(n) analytically so as to minimize the numerical errors.

Both the number of terms in arrays F_b and F_g were varied from 7 to 11 allowing the convergence rate to be examined. $F_b(11)$ and $F_g(11)$ were found to be less than 2.2×10^{-308} which is the smallest non-zero real value that can be handled by the computer. Hence 10 terms were used in the calculation of Equations (30 and 31). The calculated values of B and G were substituted into Equation (21) in order to get the values of admittance.

As with Model 2, in a measurement situation a Newton-Raphson technique is used to calculate the complex permittivity of the sample from the experimentally measured values of Y at each frequency of interest.

3.2 Experimental Procedures

3.2.1 Calibration

To measure the reflection coefficient of a one port device an incident signal I and its reflection from the unknown interface R should be measured separately. The measured reflection coefficient S_{11} is obtained from their ratio.

In practice this simple approach is insufficient because of imperfections in the network analyzer hardware. In accordance with network analyzer theory a measurement is prone to 3 major sources of systematic errors:

- Impedance mismatches within the system and in particular improperly matched source input impedance which re-reflects signal back to the unknown thus adding to the original incident signal.
- The separation of incident and reflected signals cannot be performed with 100% efficiency. This task is performed by means of directional couplers which have a finite directivity.
- Errors may arise from differences in the frequency response of components of the incident and reflection channels.

These inaccuracies generate 3 error terms E1, E2, and E3 that are mathematically related to the actual reflection coefficient Γ_a and the measured value Γ_m.

$$\Gamma_m = E1 + E2 \times \Gamma_a / (1 - E3 \times \Gamma_a) \qquad (35)$$

The purpose of the calibration is to determine these errors at each frequency of interest and to use these values to obtain the actual reflection coefficient of the unknown. These values are found by measuring the response of at least three independent standards whose

characteristics are known at all frequencies. The most commonly used standards are a short, an open, and matched loads to correct for source match, directivity and frequency response.

Details of the calibration procedure are in the Instruction manual of the network analyzer (16).

When open-ended coaxial probes are used for measurements of the dielectric properties of materials, small changes in relatively high complex reflection coefficients should be precisely measured, thus the exact calibration of the measuring system becomes a foreground problem. Ideally the calibration should be performed at the measuring plane, namely, the functional end of the measuring probe. In this case factory standards cannot be used.

There are essentially two ways of calibrating such a system:

- Calibration standards in the form of liquids of well-known dielectric properties may be used in conjunction with a valid probe admittance model.
- Alternatively, the calibration may be performed using factory standards before connecting the probe. A probe is then connected at the calibration port and the reference plane of the measurement defined by shorting the end of the probe and adjusting the electrical delay until the reflection from the short circuit at the functional end of the probe exhibits a constant 180^{0} phase angle. Under these conditions the network analyzer is fully calibrated except for the reflection from the connector of the probe.

The advantages of the first technique must be weighed against the uncertainties in the reflection coefficient of the standards which depend on the purity of the liquid, confidence interval of the dielectric parameters, dielectric model, and the impedance model of the functional end of the probe.

While the admittance model is being assessed it is not appropriate to use it to calibrate the network analyzer. Therefore, during the testing of the models the latter technique was adopted.

3.2.2 Experimental setup

The experimental setup is shown in Figure 10 . The setup comprises an HP8720 network analyzer incorporating its own scattering parameters test set, an HP9000 computer running Basic 5.1 and peripheries, a contact coaxial probe suitable for insertion into a temperature-controlled environment.

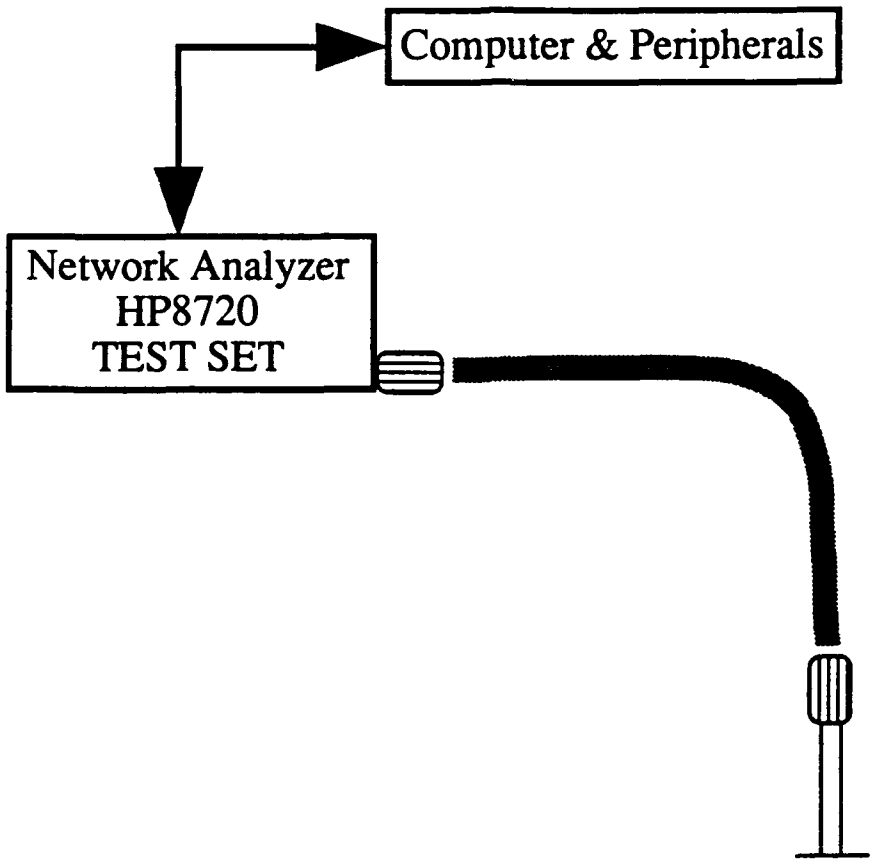

Figure 10. Experimental setup for dielectric measurements using a coaxial probe.

4. RESULTS

4.1 Comparative Study of the Three Admittance Models

The admittance of the probe was calculated at a frequency range from 130 MHz to 20 GHz using the 3 models introduced in Section 3. The results are given in Figures 11 and 12 for a 50 Ω Teflon-filled coaxial probe (3.5 mm OD, a = 0.456 mm, b = 1.490 mm, $\varepsilon_c = 2.1$) in air and water respectively. The complex permittivity of water was generated by the Debye dispersion equation (13,14).

$$\varepsilon^* = \varepsilon_\infty + (\varepsilon_S - \varepsilon_\infty) / (1 + j\omega\tau) \qquad (36)$$

where ε_∞ and ε_s are the high and low frequency limits of the relative permittivity; τ is the relaxation time.

In Figures 11 and 12 the squares (□) represent calculations using Model 1, the stars (*) Model 2 and the crosses (+) Model 3. With the probe in air (Fig. 11) there is a fairly good agreement between all 3 models for frequencies up to 10 GHz. At higher frequencies, Model 1 deviates from the predictions of the other models. With the probe in water, the agreement between the three models extends only to 3 GHz, Model 2 and 3 agree up to 7 GHz. At higher frequencies, both the real and imaginary parts of admittance calculated from Model 2 alternate between positive and negative values (Fig. 12). Model 2 fails to converge under these conditions.

The admittance of the probe immersed in water was also measured using the experimental setup described in Section 3.2. For the purpose of these measurements the network analyzer was calibrated before fixing the probe using factory standards. Figure 13 compares the measured values with the predictions of Model 3.

A. Real part

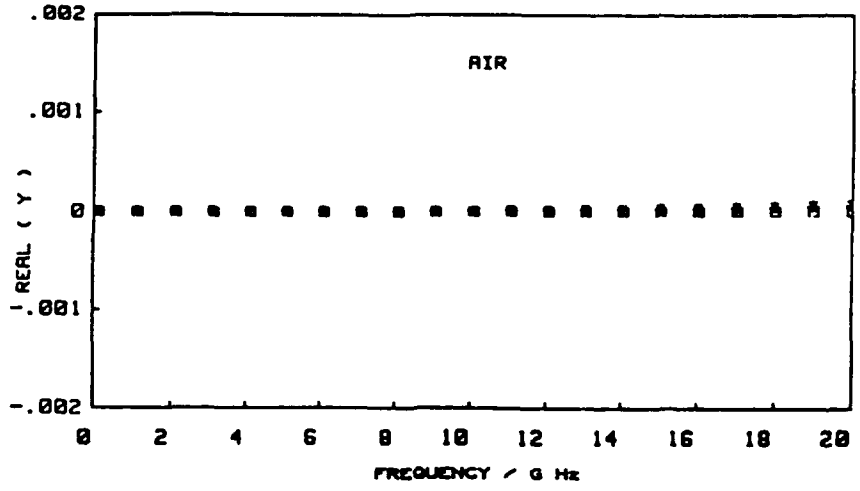

B. Imaginary part

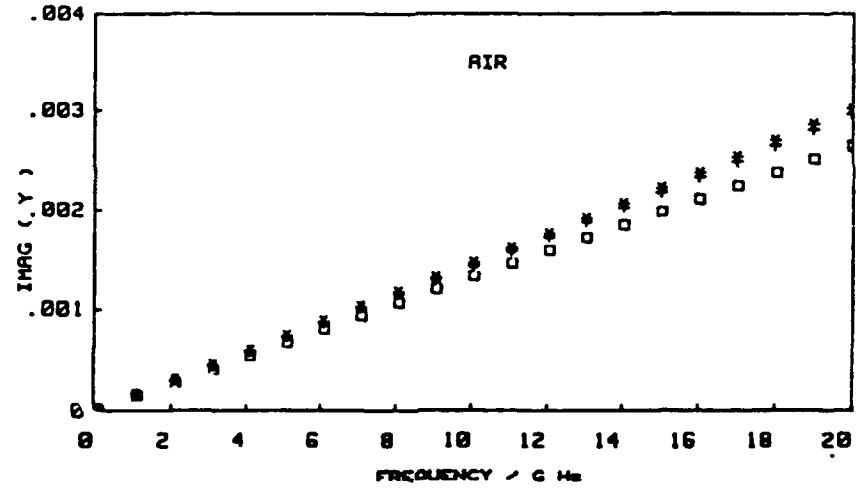

Figure 11. A Teflon-filled coaxial probe in air.

A. Real part

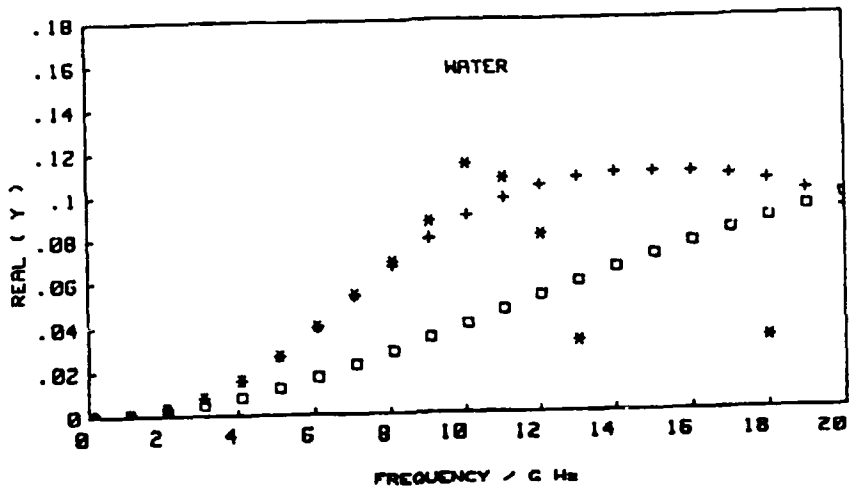

B. Imaginary part

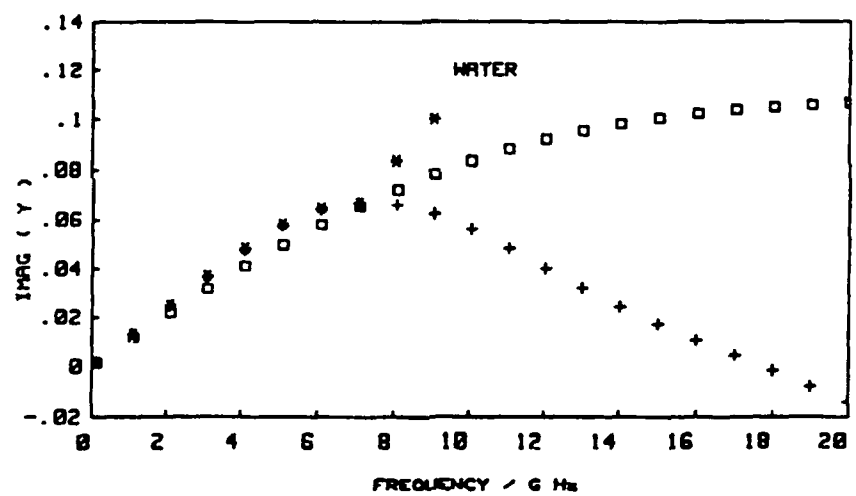

Figure 12. A Teflon-filled coaxial probe in water.

A. Measured and calculated real part.

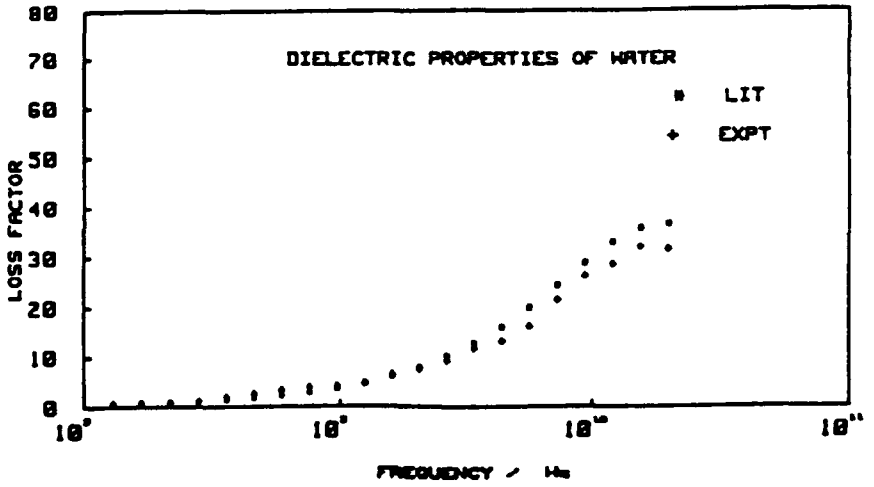

B. Measured and calculated imaginary part.

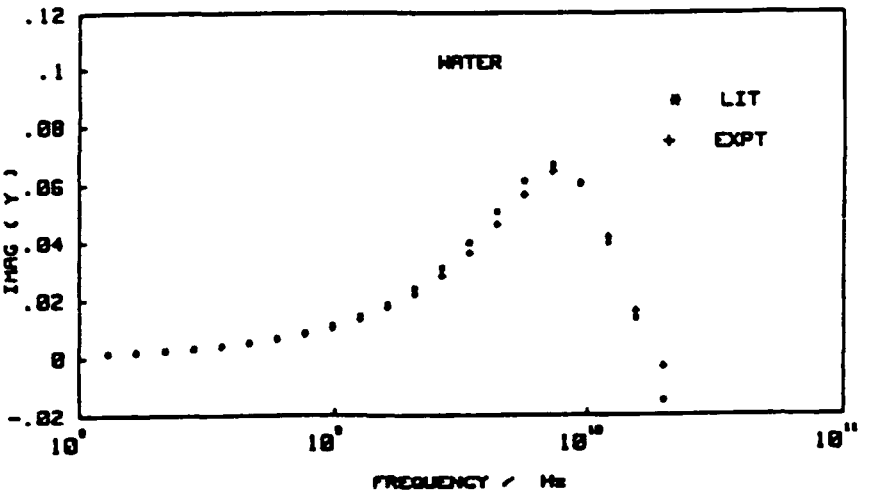

Figure 13. Comparison of the measured values.

The measurements in Figure 13 incorporate a systematic error due to multiple reflections by the uncalibrated probe connector the effect of which are to make the measured reflection coefficient to oscillate about the actual value; this effect is more apparent at high frequencies. The agreement between experimental and calculated admittance values (Fig. 13) is thus quite acceptable.

4.2 Results: Model 1

Using Model 1, good results are expected when materials of low permittivity are measured with air as reference. Equally good results are expected when aqueous systems are measured using water as reference. To test the performance of this model to the limit, a standard material of intermediate permittivity has been selected for our study.

Ethanediol has a static permittivity of ~42 at 20 °C which is intermediate between the static permittivity of water (80.1) and that of air. Moreover, the dielectric properties of ethanediol are well characterised as a function of frequency and temperature . Its dielectric dispersion is simulated by a Cole-Davidson model

$$\varepsilon^* = \varepsilon_\infty + (\varepsilon_S - \varepsilon_\infty) / (1 + j\omega\tau)^\beta \qquad (37)$$

At 20 °C ε_S, the static permittivity, is 41.4, ε_∞, the infinite permittivity, is 3.7, τ, the relaxation time, is 164.5 ps and β, the distribution parameter, is 0.8.

Fig. 14 shows the complex permittivity of ethanediol measured with air as a reference. The solid line represents the literature values.

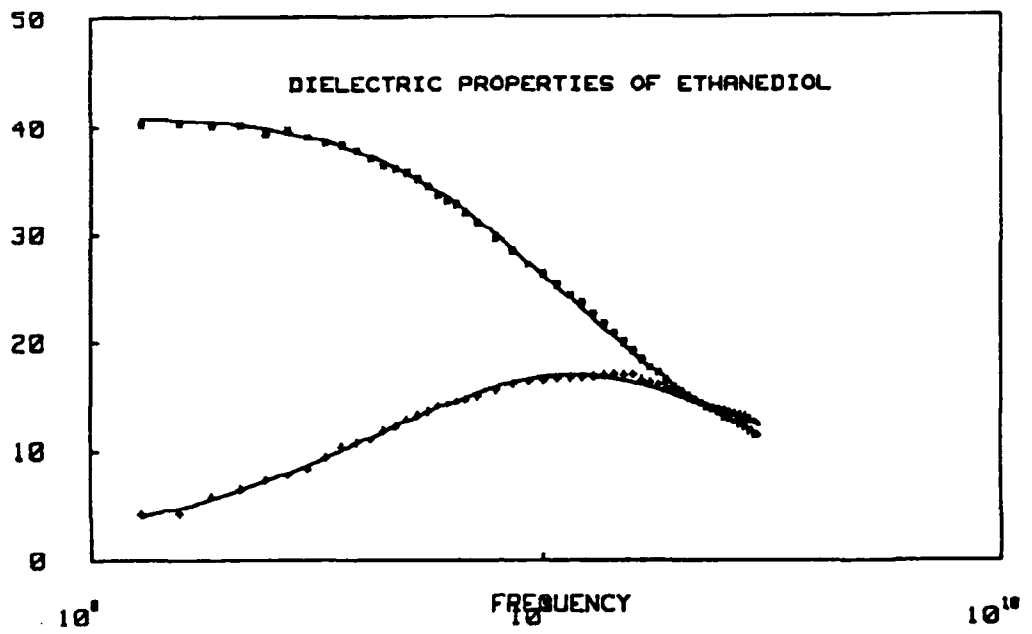

Figure 14. Dielectric properties of ethanediol at 20 °C.

4.3 Results: Model 2 and 3

Model 2 offers no advantages over either 1 of the 2 other models. Model 2 derivation was a useful comparative excercise that helped demonstrate the suitability of Model 3. Measurements reported in this section (Fig. 15 to 19) were obtained using this model on ethanol (17), methanol (18), ethanediol (19), formamide (18)and a 1% potassium chloride solution (20). These materials exhibit a dielectric behaviour described by the Debye model (Eq. 36), the Cole-Davidson variation (Equation 37) or by the Cole-Cole model:

$$\varepsilon^* = \varepsilon_\infty + (\varepsilon_S - \varepsilon_\infty) / (1 + (j\omega\tau)^{(1-\alpha)}) \qquad (38)$$

An additional conductivity term, $(j\sigma/\omega\varepsilon_0)$ where ε_0 is the permittivity of free space, is required when analysing the behaviour of materials with significant ionic conductivity. In Figures 15 to 19 the solid line represents the best fit of the data to the appropriate dielectric model (Equations 36 to 38). The parameters are given, with the 95% confidence deviation in parentheses, they all fall well within the values quoted in the literature.

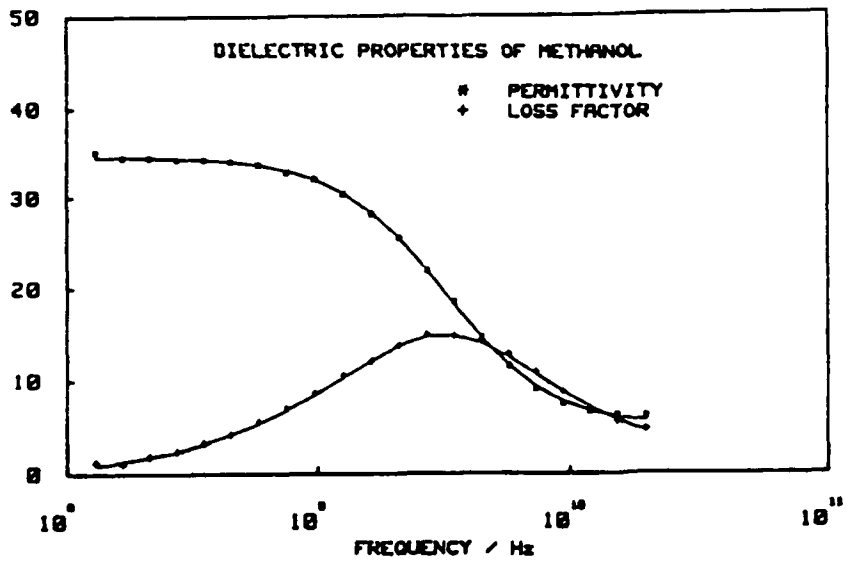

Figure 15. Dielectric properties of Methanol at 22 °C. The solid line represents Eq. (38) $\varepsilon_S = 34.6(0.1)$, $\varepsilon_\infty = 4.9(0.2)$, $\tau = 15.7(0.06)$ ps and $\alpha = 4.60.036(0.003)$.

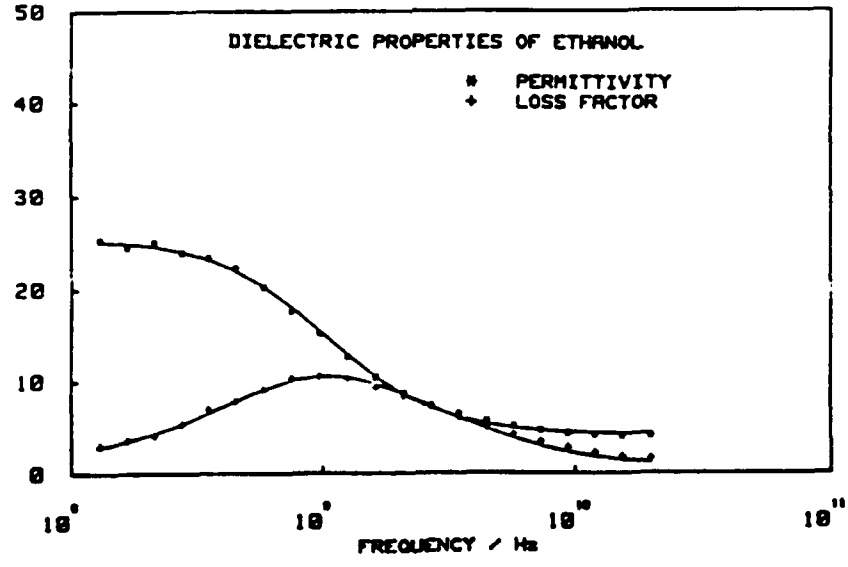

Figure 16. Dielectric properties of Ethanol at 22 °C. The solid line represents Eq. (36) with $\varepsilon_S = 25.1(0.2)$, $\varepsilon_\infty = 4.1(0.1)$, $\tau = 152(0.03)$ ps.

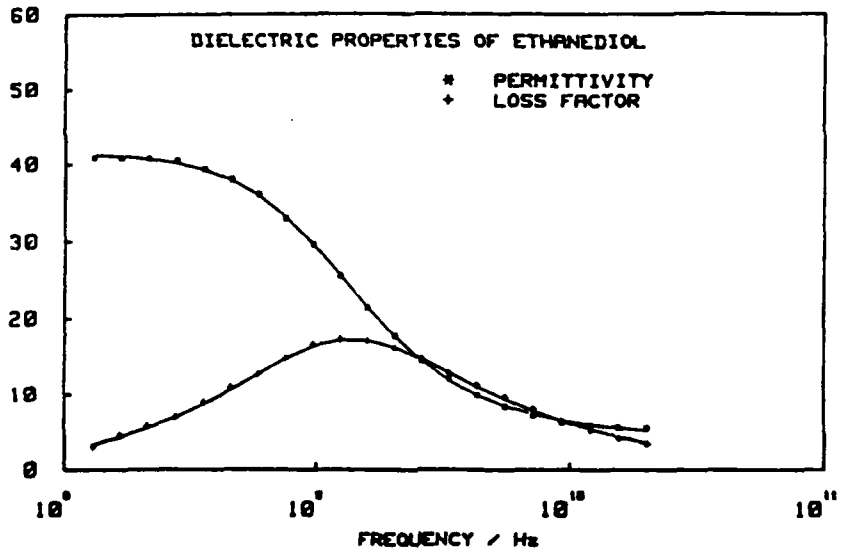

Figure 17. Dielectric properties of Ethanediol at 22 °C. The solid line represents Eq.(37) ε_S =41.6(0.1, ε_∞ = 3.8(0.2), τ = 134 ps and β = 0.082(0.01).

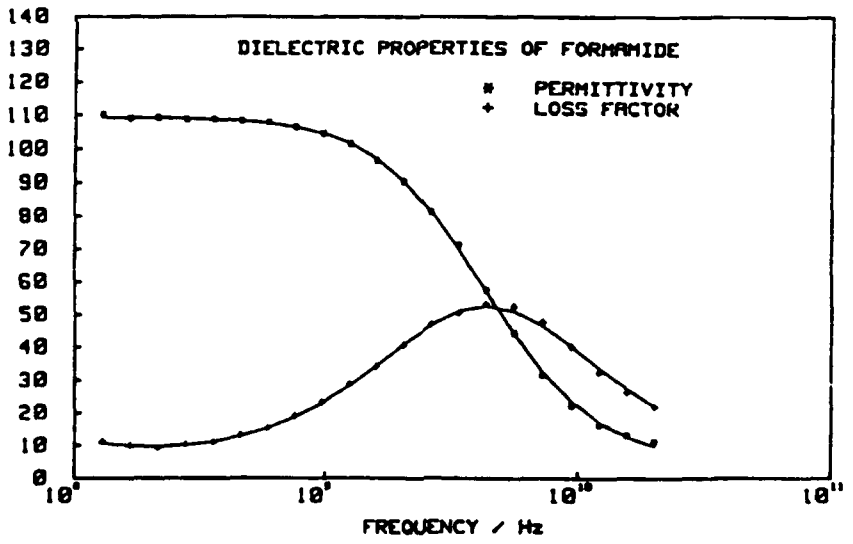

Figure 18. Dielectric properties of Formamide at 22 °C. The solid line represents Eq.(36) ε_S =109.5(0.2), ε_∞ = 6.9(0.02), τ = 37.4(0.01) ps and α = 0.052(0.003) S/m.

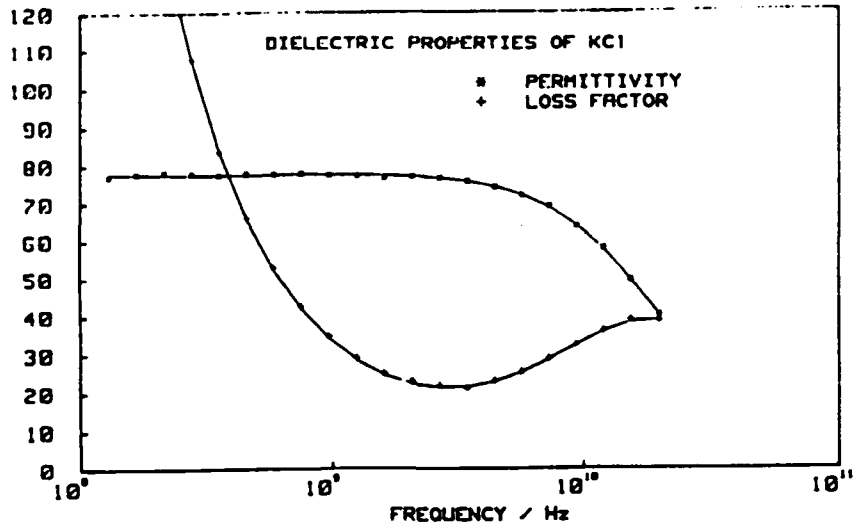

Figure 19. Dielectric properties of 1% KCl solution at 22 °C. The solid line represents Eq.(36) with ε_s =77.7(0.2), ε_∞ = 3.7(1.43), τ = 8.14(0.02) ps and α = 0..64(0.004).

4.4 Error Analysis

The errors associated with dielectric measuring techniques fall into 2 main categories: (1) hardware errors, and (2) errors originating from the admittance model. The strength of our approach is that these 2 types of errors were dealt with independently. For instance, hardware errors were corrected using the manufacturers calibration technique using standards unrelated to the admittance model. The most appropriate admittance model for the probes and frequency range covered was objectively selected. Then the measuring technique was greatly improved by combining this model into the hardware calibration. The results (Figs. 15-19) proclaim the success of this approach by showing measurements performed on liquids of known dielectric properties. In these results the measured values are mostly within 1% of the calculated values. We note, however, that the uncertainties in ε^* depend not only on the uncertainties in Γ at the measurement frequency, but also on the partial derivatives of ε^* with respect to Γ which in turn depend on the value of Γ and hence on the probe and sample properties. This complex situation is illustrated by plotting Γ at a given frequency, in the complex permittivity plane (Fig.

20). Regions of closely packed contours correspond to large partial derivatives and, therefore, good measurements resolution. The use of such mappings serves to assess the measurement problem and provides criteria for the selection of a probe for the sample permittivity and frequency range required.

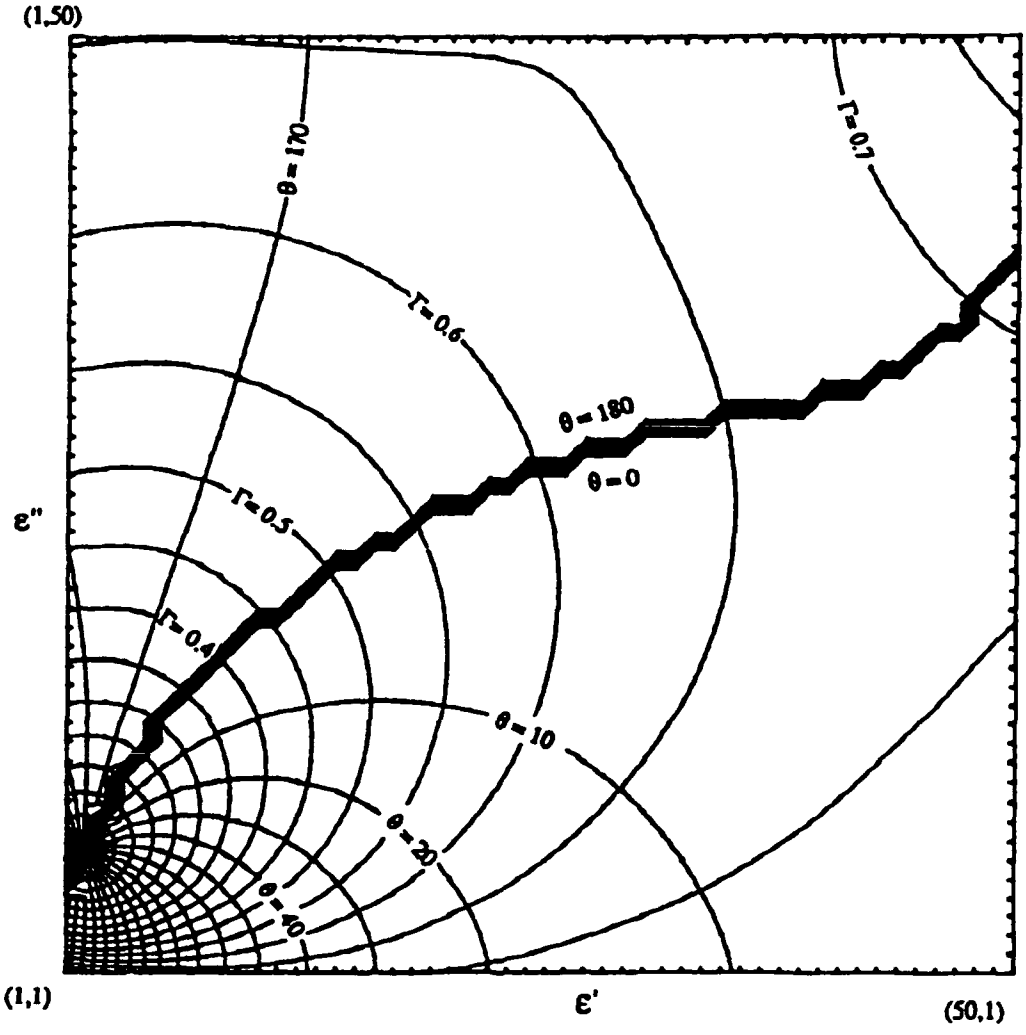

Figure 20. Mapping of G in the ε* plane (Model 3, 3 mm probe at 20 GHz).

5. CONCLUSIONS

The work reported in Section 2 shows that the finite element technique is well suited to the study of the fringing fields of coaxial probes. Although a similar approach has previously been used to calculate the end of line capacitance, this is the first time it is used to map equipotential lines. This approach was made possible by the incorporation of a newly developed automatic mesh generator for ease of application and high resolution.

The use of a coaxial probe for dielectric measurements requires the development of an end-of-line admittance model. A 3 mm, polyterrafluoroethylene (PTFE) filled probe was used in this study. The advantages and limitations of the simple lumped parameter model were illustrated. By comparing the 2 other but equivalent formulations for the admittance of the coaxial cable, Model 2 was found to fail at high frequencies (>7 GHz). This failure could be due to the nature of the exponential term in Equation 16. As frequency increases, the value of k increases and hence the frequency of vibrations of both the real and imaginary parts of this term becomes higher. When the frequency is increased beyond a certain limit, the vibration is so rapid that it becomes meaningless to do the integration on this term. Model 3 was found to be a better approximation for admittance of the coaxial probe in contact with lossy media for the frequency range 130 MHz to 20 GHz.

The work covered by our report forms the first stage in an in-depth study of dielectric measurements using contact coaxial probes. This work inspires further study involving:

1. Coaxial probe field penetration in lossy media;
2. Measurements on finite thickness samples;
3. Measurements on layered materials; and
4. Developments of admittance models incorporating the excitation of TEM and higher order modes at the probe-sample interface.

6. ACKNOWLEDGMENTS

This work is the result of a team effort by members of Professor E.H.Grant's Dielectrics Research Group at King's College. I would especially like to mention Miss A. Chan who has contributed significantly to the success of this programme.

Thanks are also due to Mr. J.C.Toler of the Georgia Institute of Technology, Atlanta, Georgia for his help and patience in the technical and financial management of this project.

7. REFERENCES

1. Burdette, E.C., F.L. Cain, and J. Seals. *In vivo* probe measurement technique for determining dielectric properties at VHF through microwave frequencies, IEEE trans Microwave Theory Tech, **MTT-28**: 414-427 (1980).

2. Gabriel, C., E.H. Grant, and I.R. Young. Use of time domain spectroscopy for dielectric measurements with a coaxial probe, J Phys E: Sci Instrum, **19**: 843-846 (1986).

3. Marsland, T.M., and S. Evans. Dielectric measurements with an open-ended coaxial probe. Proc IEE **134:** 341-349 (1987).

4. Gabriel, C., and E.H. Grant. Dielectric sensors for industrial microwave measurements and control. Proc High Frequency/Microwave Processing and Heating KEMA Conference, Arnhem, Netherlands, 1989.

5. Mosig, J.R., J.C.E. Besson, M. Gex-Fabry, and F.E. Gardiol. Reflection of an open-ended coaxial line and application to nondestructive measurement of materials. IEEE Trans Instrum Meas **IM-30**: 41-46 (1981).

6. McArthur, P. Numerical analysis of open-ended coaxial probes and its application to *in-vivo* dielectric measurements. Ph.D. Thesis, King's College, University of London, 1989.

7. Misra, D.K. A quasi-static analysis of open-ended coaxial lines. IEEE Trans Microwave Theory Tech **MTT-35**: 925-928 (1987).

8. Marcuvitz, N. *Wavelength Handbook*, pp. 213-216. New York: McGraw-Hill, 1951.

9. Levine, H.R., and C.H. Papas. Theory of circular diffraction antenna, J Appl Phys, **22**: 29-43 (1951).

10. Xu, D., L. Li, and Z. Jiang. Measurement of the dielectric properties of biological substances using an improved open-ended coaxial line resonator method. IEEE Trans Microwave Theory Tech **MTT-35**: 1424-1428 (1987).

11. Misra, D., M. Chabbra, B.R. Epstein, M. Mirotznik, and K.R. Foster. Noninvasive electrical characterisation of materials at microwave frequencies using an open-ended coaxial line: Test of an improved calibration technique. IEEE Trans Microwave Theory Tech **MTT-38**: 8-14 (1990).

12. Abramowitz, M., and I.A. Stegun. *Handbook of Mathematical Functions*. New York: Dover Publications, Inc., 1965.

13. Grant, E.H., R.J. Sheppard, and G.P. South. Dielectric Behaviour of Biological Molecules in Solution. Oxford: Oxford University Press, 1978.

14. Malmberg, C. and Maryott. Dielectric constant of water from 0 - 100 °C, J. Res. **NBS 56** (1): 1-6 (1956).

15. Grant, E.H., T. Buchanan, and H. Cook. Dielectric behaviour of water at microwave frequencies. J Chem Phys **26** (1): 156-161 (1957).

16. System Operation and Programming Manual: HP8720A Microwave Network Analzyer, Hewlett Packard, Part No. 08720-90002.

17. Szwarnowski, S. Ph.D. thesis, London University, 1979.

18. Jordan, B.P., R.J. Sheppard, and S. Szwarnowski. The dielectric properties of formamide ethanediol and methanol. J Phys D: Appl Phys **11**: 695-701 (1978).

19. Levin, V.V., and T.L. Podlovchenlco. Dispersion of the dielectric permeability of Ethylene Glycol, translated from Zhurnal Strukturnoi Khimii, **11** (4): 766-767 (1970).

20. Hasted, J.B. *Aqueous Dielectric*. London: Chapman and Hall, 1973.